Koskinen, Tomi; Khayrudinov, Vladislav; Emadi, Fahimeh; Jiang, Hua; Haggren, Tuomas; Lipsanen, Harri; Tittonen, Ilkka

Thermoelectric Characteristics of InAs Nanowire Networks Directly Grown on Flexible Plastic Substrates

Published in:
ACS Applied Energy Materials

DOI:
10.1021/acsaem.1c03405

Published: 27/12/2021

Document Version
Publisher's PDF, also known as Version of record

Please cite the original version:
Koskinen, T., Khayrudinov, V., Emadi, F., Jiang, H., Haggren, T., Lipsanen, H., & Tittonen, I. (2021). Thermoelectric Characteristics of InAs Nanowire Networks Directly Grown on Flexible Plastic Substrates. *ACS Applied Energy Materials*, *4*(12), 14727–14734. https://doi.org/10.1021/acsaem.1c03405

ACS APPLIED ENERGY MATERIALS

www.acsaem.org Article

Thermoelectric Characteristics of InAs Nanowire Networks Directly Grown on Flexible Plastic Substrates

Tomi Koskinen,* Vladislav Khayrudinov, Fahimeh Emadi, Hua Jiang, Tuomas Haggren, Harri Lipsanen, and Ilkka Tittonen

Cite This: *ACS Appl. Energy Mater.* 2021, 4, 14727−14734

Read Online

ACCESS | Metrics & More | Article Recommendations | Supporting Information

ABSTRACT: III-V semiconductor nanowires have shown promise for thermoelectric applications, but their use in practical devices has conventionally been hindered by complex fabrication processes and device integration. Here, we characterize the thermoelectric properties of InAs nanowire networks directly grown on flexible polyimide plastic. The n-type nanowire networks achieve a high room-temperature Seebeck coefficient of $-110.8\ \mu\text{V K}^{-1}$ and electrical conductivity of $41\ \text{S cm}^{-1}$, resulting in a thermoelectric power factor of $50.4\ \mu\text{W m}^{-1}\ \text{K}^{-2}$. Moreover, the nanowire networks show remarkable mechanical flexibility with a relative change in resistance below 0.01 at bending radii below 5.2 mm. We further establish the thermoelectric performance of InAs nanowire networks on plastic using a facile proof-of-concept thermoelectric generator producing a maximum power of 0.44 nW at a temperature gradient of 5 K. The findings indicate that direct growth of III-V nanowire networks on plastic substrates shows promise for the development of flexible thermoelectrics applications.

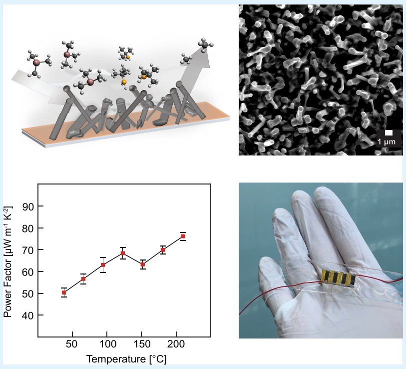

KEYWORDS: *indium arsenide, III-V, nanowire, thermoelectric, flexible, MOVPE*

1. INTRODUCTION

III-V semiconductor nanowires constitute a platform for rich physical phenomena with characteristics such as low electron effective mass, exceptional charge carrier mobility, as well as efficient light absorption and emission made possible by the direct band gap.[1] These properties have resulted in a range of applications in areas including high-speed electronics,[2,3] optoelectronics,[4−6] spintronics,[7] and quantum computing devices.[8,9] Furthermore, nanowires have been theoretically shown to possess enhanced thermoelectric performance over that of bulk due to altered electron density-of-states (DOS) and phonon confinement induced by reduced dimensionality,[10,11] subsequently improving the unitless thermoelectric figure-of-merit $zT = S^2\sigma T\kappa^{-1}$, where S, σ, κ, and T denote the Seebeck coefficient, electrical conductivity, thermal conductivity, and temperature, respectively. Recently, several experimental studies have shown superior thermoelectric performance in semiconductor nanowires compared to bulk[12−16] resulting from substantial increases in the Seebeck coefficient with a simultaneous decrease in thermal conductivity resulting from phonon confinement.

The Seebeck effect presents a clean and reliable way of directly converting heat into electricity with possible applications in, for example, harvesting of waste heat, various distributed sensors, as well as power generation for wearable electronics. Conventional thermoelectric generators exploiting the effect consist of n- and p-type bulk semiconductor blocks, resulting in rigid and nonflexible devices. Consequently, their performance is limited in applications lacking a conformal contact between the heat source and the generator due to the resulting suboptimal thermal gradient, which ultimately leads to reduced power density. The importance of proper thermal contact is elevated in low-grade heat applications, such as medical sensors and similar wearable devices, where the available contact area is restricted and temperature gradients are small.[17,18] Introducing thermoelectric generators as power sources in such applications therefore requires solutions combining high thermoelectric efficiency and a flexible form factor.[17,19]

While inorganic semiconductors typically show impressive thermoelectric characteristics, their use in flexible applications is often hindered by their inherently rigid and brittle composition leading to device failures. The brittleness can, however, partially be alleviated by exploiting the structural properties of nanostructures such as bottom-up synthetized nanowires. We have recently shown that III-V semiconductor nanowires can be directly grown on flexible polyimide substrates using metalorganic vapor phase epitaxy (MOVPE).[20] From the flexible application perspective, this

Received: October 29, 2021
Accepted: November 17, 2021
Published: November 29, 2021

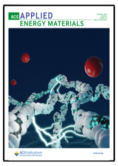

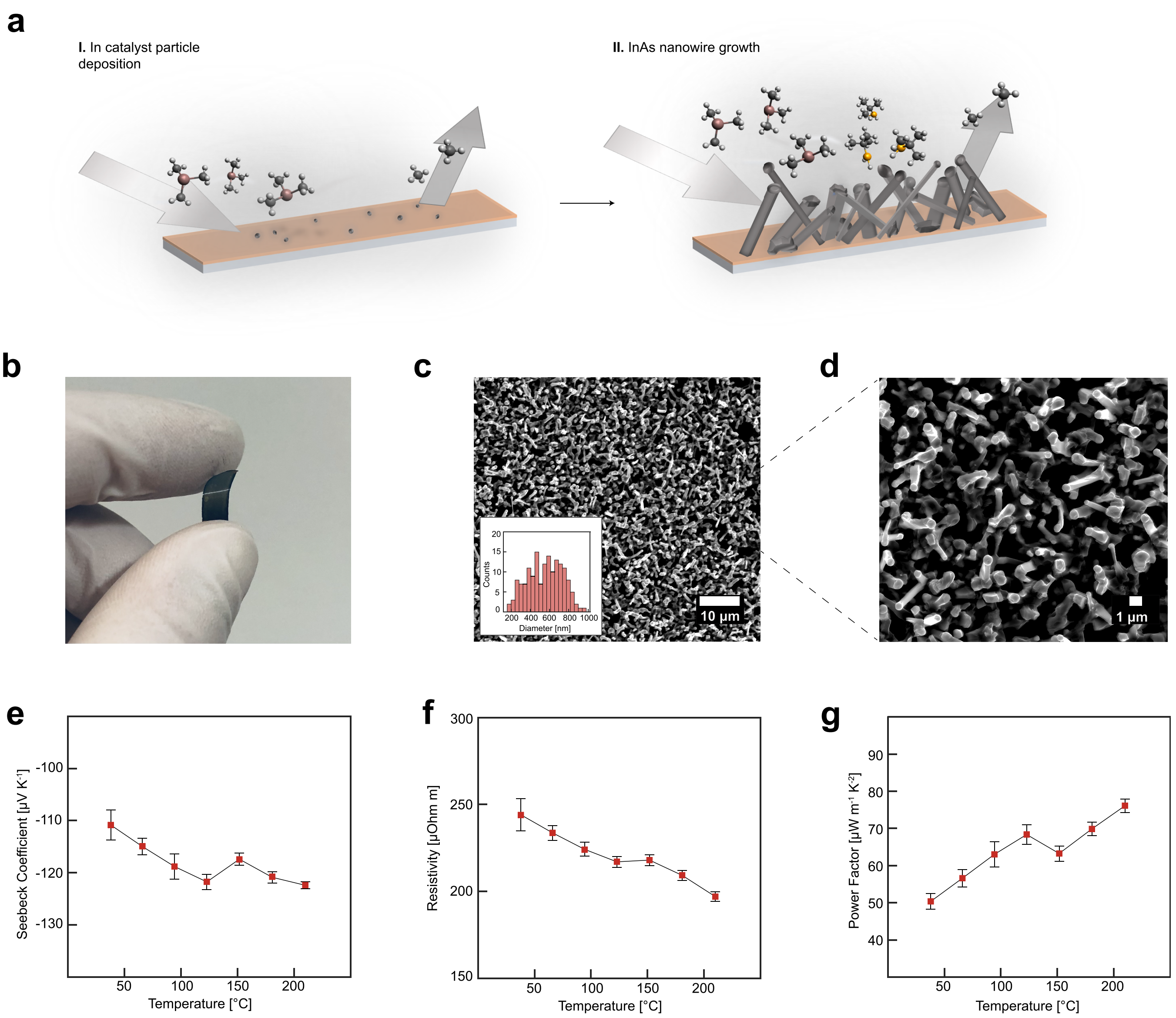

Figure 1. (a) Process schematic showing the two major steps in the nanowire growth process. (b) Photograph of the InAs nanowire network directly grown on the flexible polyimide film. (c) SEM micrograph of the InAs nanowire network showing the overall morphology of the structure. Inset: diameter distribution of the nanowire network. (d) SEM image showing the morphology of nanowires constituting the network. (e) Seebeck coefficient, (f) electrical resistivity, and (g) thermoelectric power factor in the temperature range 30−210 °C.

approach has various benefits. First, it avoids complicated transfer steps often required by nanowires grown on rigid substrates. Second, due to the small interfacial area between the nanowire base and the substrate, lattice mismatch-induced stress is low and high crystalline quality associated with bottom-up growth processes can be attained despite the amorphous nature of the plastic substrate. Moreover, the polyimide plastic is less expensive, lighter in weight, and mechanically more robust than conventional substrates. Contrary to what is characteristic to vertical nanowire arrays, III-V nanowires grown on polyimide form percolative, electrically conductive networks, thus enabling continuous film-like structures of a considerably large area and, on the other hand, remarkably alleviating the deposition of electrical contacts.

Here, we report the thermoelectric characteristics of InAs nanowire networks directly grown on heat-resistant polyimide films. Our approach allows combining the prominent thermoelectric performance of the inorganic semiconductor nanowires with the functional properties of the flexible plastic substrate, resulting in a facile and inexpensive route for producing flexible III-V nanowire thermoelectric devices. The characterization results show that InAs nanowire networks grown at 460 °C reach a maximum thermoelectric power factor PF = $S^2\sigma$ of 50.4 μW m^{-1} K^{-2} at room temperature. The networks show excellent stability during tensile bending with a relative change in resistance below 0.01 at 5.2 mm bending radius. Finally, we demonstrate a flexible thermoelectric generator comprising four n-type legs producing an output power of 0.44 nW at a temperature gradient of 5 K.

2. RESULTS AND DISCUSSION

2.1. Nanowire Growth and Morphology. InAs nanowires were synthesized on polyimide in an MOVPE reactor using a vapor−liquid−solid (VLS) growth process reported earlier.[20] The two major steps in the growth process have been illustrated in a process schematic presented in Figure 1a. Briefly, In catalyst droplets were deposited *in situ* on the polyimide substrate, after which InAs nanowires were grown under trimethylindium (TMIn) and tertiarybutylarsine (TBAs) flows. Further details and detailed growth parameters are described in the experimental section. The VLS growth process results in dense and continuous nanowire networks that are dark gray in color, as presented in Figure 1b.

The morphology of the nanowire networks was characterized with scanning electron microscopy (SEM). SEM images in Figure 1c,d show the overall disordered morphology of the nanowire network. As witnessed previously,[20] the nanowires nucleated from In droplets grow in all directions, forming a dense network consisting of nanowires of varying diameters and lengths. Based on a statistical analysis including 234 observations from SEM images, the mean nanowire diameter is 543 nm with a standard deviation of 177 nm. The diameter distribution is further visualized in the inset of Figure 1c, showing a roughly normally distributed shape.

Additional insight on the structural characteristics is gained via high-resolution transmission electron microscopy (HRTEM) and energy dispersive X-ray spectroscopy (EDS) analysis as presented in Supporting Information, Figure S1. The HRTEM micrographs confirm that the studied nanowires have a highly crystalline structure in the zinc blende configuration, as further evidenced by the spot diffraction pattern. Investigation of nanowire edges shows that the surfaces are relatively clean with no clear evidence of an oxide layer, although the EDS mapping shows a faint signal of O that could originate from the native oxide. The mapping and the EDS spectrum obtained from the center of the nanowire confirm that the composition corresponds to InAs.

To obtain the electronic transport parameters, a rough approximation is made to treat the nanowire network as a thin film of thickness equal to the average height of the network. The height of the network perpendicular to the substrate is evaluated from crosscut SEM images, as presented in Supporting Information, Figure S2. The cross-section SEM images were then analyzed with ImageJ, showing an average network height of 1.67 μm.

2.2. Thermoelectric and Electronic Transport Properties.

After the growth, the nanowire network samples were prepared for electrical and thermoelectric characterization by depositing Ti/Au contact pads to improve the electrical contact. The thermoelectric properties were then characterized in the temperature range of 30−210 °C in an inert helium atmosphere, and the Seebeck coefficient and electrical conductivity were measured with the sample grown on polyimide attached onto a glass support piece. The Seebeck coefficient, electrical conductivity, and resulting power factor as a function of temperature are presented in Figure 1e−g. At room temperature, the InAs nanowire network shows a favorable Seebeck coefficient of $-110.8\ \mu\mathrm{V\ K^{-1}}$, aligning to the same range as in previous reports for single InAs nanowires,[21−23] with the absolute value showing an increasing trend as a function of temperature and reaching $-122.4\ \mu\mathrm{V\ K^{-1}}$ at 210 °C. The rather unanticipated kink taking place at approximately 150 °C is reproducible across different measurements and similar samples, but the mechanism causing it is not evident. However, based on the rather abrupt change observed in Figure S3 presented in the Supporting Information, a possible explanation for the behavior could be thermally activated trap states formed at grain boundaries and other similar defects in the structure. Such defects emerging from the mixing of wurtzite and zinc blende crystal phases are expected to occur frequently in the network with a typical example presented in the TEM micrograph of Figure S1d in the Supporting Information.

In comparison to bulk, the Seebeck coefficient is typically improved in nanowire systems due to the reduced dimensionality that results in sharp features in the electron DOS. However, the nanowires studied here have a large mean diameter of 543 nm, which effectively excludes electron confinement effects.[24] Yet, the Seebeck coefficient observed here reaches a magnitude similar to those obtained from nanowires of smaller diameter, implying that such effects are likely not playing an important role in the thermoelectric performance of InAs nanowire systems such as those presented in this work.

The nanowire networks show low electrical resistivity without any intentional doping. In previous reports studying InAs nanowires, low electrical resistivity is typically attributed either to the formation of an electron accumulation layer at the nanowire surfaces or to unintentional doping caused by residual impurities from the growth process. The first mechanism results in Fermi level pinning, i.e., bending of the conduction band at the nanowire surface, which fixes the position of the Fermi level above the conduction band minimum.[25,26] This phenomenon has been proposed to arise due to surface oxidation,[27] native In adatom defects, hydrogen impurities,[28] or surface excess As atoms.[26] Since the nanowire networks investigated in this work are brought to ambient in between the growth procedure and the thermoelectric measurements, the formation of a native oxide layer on the nanowire surfaces would be a reasonable explanation for the observed low resistivity.[27,29] However, despite the EDS mapping showing a faint O signal as presented in Figure S1, Supporting Information, the nanowire surfaces show no clear signatures of a native oxide.

We gather complementary insight on the electronic transport properties by obtaining the charge carrier concentration and mobility by Hall mobility measurement in the van der Pauw geometry. The measurement at room temperature results in a charge carrier concentration value of $n = -7.76\cdot 10^{18}\ \mathrm{cm^{-3}}$ and Hall mobility $\mu = 93.6\ \mathrm{cm^2\ V^{-1}\ s^{-1}}$, thus yielding an electrical conductivity value of the same order of magnitude as obtained in the thermoelectric measurements. The charge carrier concentration is considerably higher than what is encountered for intrinsic bulk InAs,[30] which suggests the existence of incorporated donors. Since the growth process does not include the introduction of any doping agents, the moderate charge carrier concentration is likely to be at least partially caused by unintentional dopant incorporation taking place in the process. Previous investigations on the topic have hinted that the growth temperature, V/III ratio, and choice of precursors affect the charge carrier concentration,[31−33] with decreasing temperature and V/III ratio together with TMIn precursor typically resulting in higher charge carrier concentration, the origin of which has been attributed to carbon incorporation. As an example, in MOVPE-grown InAs nanowires, a charge carrier concentration of $6.2\cdot 10^{17}\ \mathrm{cm^{-3}}$ has been obtained using TMIn precursor with a V/III ratio of 160 and growth temperature of 450 °C.[32] The V/III ratio used in our process is significantly lower than what was reported in the cited works, implying that even stronger carbon incorporation is likely to take place. The temperature

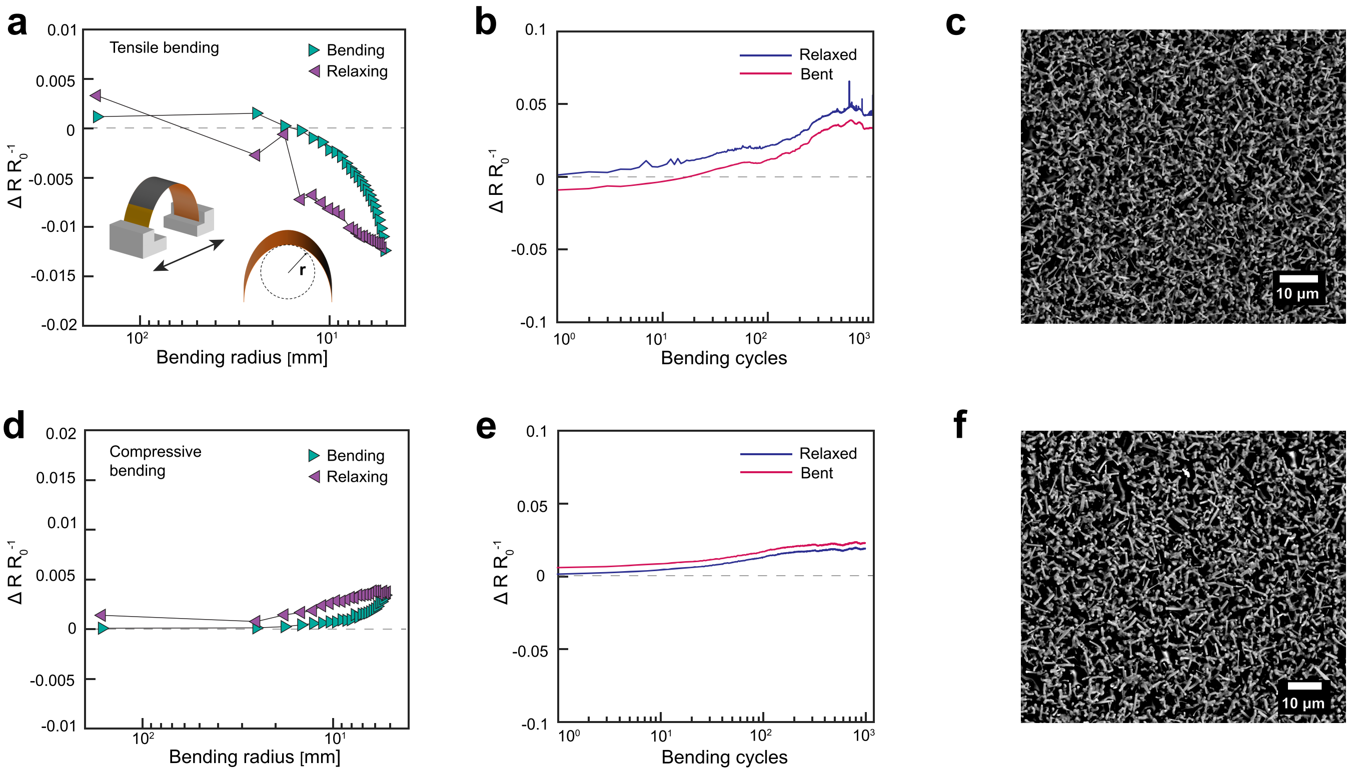

Figure 2. (a, d) Relative change in resistance under (a) tensile and (b) compressive stress as a function of bending radius. (b, e) Relative change in resistance as a function of consecutive (b) tensile and (e) compressive bending cycles. (c, f) SEM images of the nanowire networks after 1000 (c) tensile and (f) compressive cycles.

dependence of electrical resistivity is similar to that of the Seebeck coefficient, showing a decreasing trend with increasing temperature in the studied range, which is a clear signature of non-degenerate doping and semiconducting character.

The obtained Seebeck coefficient and electrical conductivity result in a thermoelectric power factor ranging from 50.4 μW m^{-1} K^{-2} at room temperature to 76.6 μW m^{-1} K^{-2} at 210 °C. The temperature-dependent data show a kink deviating from the overall trend at 150 °C resulting from similar deviations in both the Seebeck coefficient and electrical resistivity. The values obtained for electrical conductivity and Seebeck coefficient can be further used to roughly evaluate the electronic contribution to thermal conductivity using the Wiedemann−Franz law $\kappa_e = \sigma LT$, in which the Lorenz coefficient can be adjusted to properly describe the electronic properties in nondegenerate semiconductors by $L = 1.5 + \exp(|S|/116)$,[34] resulting in $L = 1.88 \cdot 10^{-8}$ WΩ K^{-2} using the Seebeck coefficient value obtained at room temperature. Thus, we obtain the electron contribution to thermal conductivity amounting to $\kappa_e = 0.023$ W m^{-1} K^{-1}. This value is rather low and implies that the major part of thermal conduction in the structure takes place due to the lattice contribution of thermal conductivity $\kappa_l = \kappa_{tot} - \kappa_e$, where κ_{tot} is the total thermal conductivity. The result underscores that the electronic and thermal transport in the network structure appears to be quite disconnected, which is extremely important in obtaining high thermoelectric performance.

2.3. Flexibility and Mechanical Stability. The mechanical flexibility of the nanowire networks is studied by measuring the relative change in the network electrical resistance during controlled bending of the polyimide substrate.[35] The setup used to bend the sample is illustrated in the inset of Figure 2a. Intriguingly, the InAs nanowire networks grown on polyimide withstand bending extremely well up to a low bending radius of 5.2 mm, as presented in Figure 2a. Moreover, unlike what is typical to conventional thin films, the nanowire networks show negative relative change in resistance during tensile bending, indicating improved electrical contact between adjacent nanowires in the network. On the contrary, when a similar sample is placed upside down for compressive bending, the sample resistance shows increasing behavior as a function of increasing bend radius with the relative change of resistance still staying well below 0.01 at a bending radius of 5.2 mm as presented in Figure 2d. In both experiments, the observed relative change of resistance as a function of bending to lower radii is largely reverted when the film is again released to a neutral position, indicating that the network structure stays largely unaffected by both tensile and compressive stress characteristic to bending.

To further evaluate the structural stability of the nanowire networks, the samples are consecutively bent to a low bending radius of 5.2 mm 1000 times while recording the resistance at both zero and extreme positions. The nanowire networks show stable performance in both tensile and compressive directions with an increase in the relative change of resistance below 5% after the cycles, as shown in Figure 2b,e. Figure 2c,f shows SEM micrographs of the two samples after the repeated bending cycles. The samples are imaged at a tensile radius of ∼5.8 mm and a compressive radius of ∼6.0 mm, respectively. The micrographs do not show cracks or other visible deterioration in the nanowire network structure, thus being well in agreement with the results obtained in the consecutive bending experiment.

https://doi.org/10.1021/acsaem.1c03405
ACS Appl. Energy Mater. 2021, 4, 14727−14734

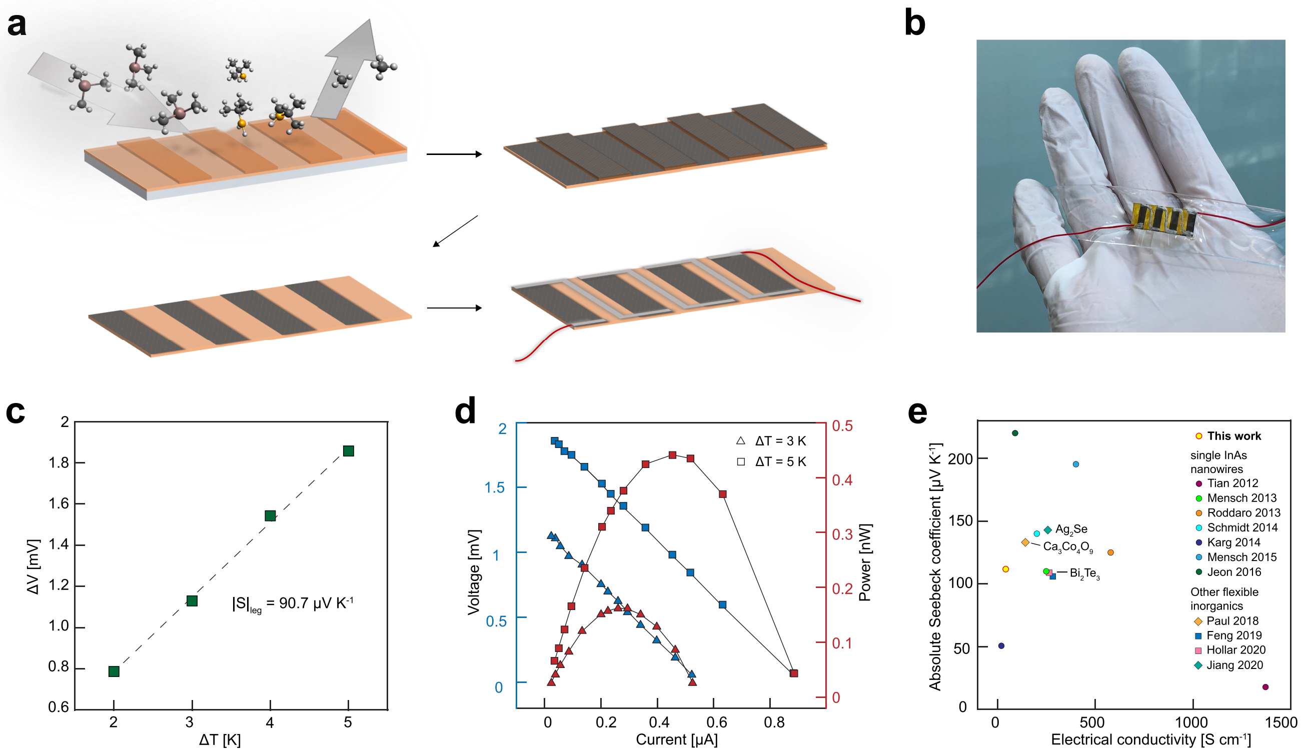

Figure 3. (a) Process of fabricating the nanowire network thermoelectric generator. The polyimide tape is fixed on a glass substrate and masked with strips of the same polyimide tape. InAs nanowires are grown on the polyimide, forming a continuous network structure. After the growth, the masking strips are removed, revealing the generator legs. The polyimide film is carefully removed from the glass substrate, and the legs are connected using flexible silver epoxy. (b) Photograph of the fabricated generator after casting into the flexible PDMS enclosure. (c) Open-circuit voltage produced by the generator as a function of applied temperature gradient. Absolute value of the Seebeck coefficient for a single leg is extracted from the linear fit. (d) Current−voltage and current−power characteristics of the generator with two different temperature gradients. (e) Comparison of the Seebeck coefficient and electrical conductivity values of the InAs nanowire network to previously reported values for single InAs nanowires[21−23,36−39] and state-of-the-art flexible inorganics.[40−43]

2.4. InAs Nanowire Network Thermoelectric Generator. The practical device performance of the nanowire networks is demonstrated by fabricating a proof-of-concept flexible thermoelectric generator. The n-type InAs nanowire network legs for the generator are fabricated in a single MOVPE run on the same substrate by masking the areas required by interconnects with polyimide tape. The fabrication process steps are illustrated in Figure 3a. After removing the masking polyimide strips after the MOVPE growth, the legs are interconnected with flexible silver epoxy and the generator is connected to the external wiring. The final generator consists of four 8 × 2 mm n-type InAs nanowire network legs directly grown on an 8 × 22 mm substrate. The generator is further sealed into a flexible PDMS enclosure to better facilitate practical device use. A photograph of the complete generator is presented in Figure 3b.

The performance of the generator is investigated by placing it on a hotplate with the hot end in contact with the hotplate surface, while the cold end is kept in ambient temperature. The temperatures at each end were monitored using external thermocouples assembled in contact with the generator. To measure the current−voltage and current−power characteristics, the generator was connected to a circuit consisting of voltage and current meters and a variable resistor load as presented in Figure S4, Supporting Information. Figure 3c shows the open circuit voltage as a function of applied temperature gradient. Current−voltage and current−power characteristics resulting from varying the load resistance at three different temperature gradients are presented in Figure 3d. At the highest tested temperature gradient of 5 K, the output power at matched load resistance equals 0.44 nW.

2.5. Discussion. To gain perspective on the thermoelectric performance of the presented InAs nanowire network on plastic, the observed room-temperature power factor is compared to existing experimental results from individual InAs nanowires[21−23,36−39] and other flexible inorganic materials representing the current state-of-the-art[40−43] in Figure 3e. At room temperature, the previously reported single InAs nanowires show |S| between 51 and 220 μV K^{-1} and σ between 20 and 1372 S cm^{-1} with the highest reported power factor value of 1.7 mW m^{-1} K^{-2} measured from a 20 nm diameter nanowire by Mensch *et al.*[21] The Seebeck coefficient observed in the nanowire networks investigated in this work falls in the middle of the reported range, while the electrical conductivity is, reasonably, lower than what is typically encountered in individual InAs nanowires. Factors impacting the result include at least the multiple interfaces between adjacent nanowires in the network that contribute negatively by introducing electron scattering. We emphasize that our results from a large-area network fall in a comparable range with values reported for single InAs nanowires, thus underlining the potential of the presented fabrication method in realizing practical large-area devices.

The obtained performance falls slightly behind that of other flexible inorganics included in the comparison, again largely due to lower electrical conductivity. The Seebeck coefficient is, nevertheless, approximately on par with recently reported results for both Bi_2Te_3 and $Ca_3Co_4O_9$. We note that the fabrication processes of many of the better-performing materials remain rather complex, whereas the reported nanowire networks can be integrated into devices without complicated transfer processes or multiple process steps.

While the thermoelectric power factor $S^2\sigma$ observed in this work shows promise in terms of further development, determining the thermal conductivity required to evaluate the figure-of-merit zT is challenging due to the complex morphology of the network structure, which practically excludes the use of 3ω or optical pump-probe thermoreflectance methods due to the difficulty of depositing the heater or transducer structures, respectively. Since the network contains a large quantity of interfaces and voids as witnessed in the SEM micrographs, phonon-interface scattering processes are presumed to strongly suppress the thermal transport, thus enhancing zT.[44] Previous studies on the thermal properties of single InAs nanowires and InAs nanowire arrays have reported thermal conductivity values ranging from below 2 up to 16 W m^{-1} K^{-1},[45−49] thus greatly falling below the bulk value. The electronic thermal conductivity value κ_e = 0.023 W m^{-1} K^{-1} obtained in this work thus amounts to only a small fraction of κ_{tot}, implying the relevance of phonon transport engineering for effectively tuning the total thermal conductivity. This further highlights the potential of large-area nanowire networks in thermoelectric power generation.

In the future, we expect the polyimide substrate growth method to translate also to other III-V semiconductor nanowire systems. In addition to the n-type InAs system studied here, this would allow the investigation of both p-type materials required by complementary thermoelectric generators and higher-performing n-type materials, such as InSb, which has previously been predicted to possess the highest thermoelectric power factor among the III-V compounds.[11] Further, introducing core−shell heterostructures could offer a pathway to increased control over both the electronic and thermal transport in the network structure.[50]

3. CONCLUSIONS

In summary, we have characterized the Seebeck coefficient and electrical conductivity of InAs nanowire networks directly grown on plastic. Moreover, we have demonstrated the mechanical flexibility of the InAs nanowire networks and further utilized the growth technique to fabricate an array of n-type legs for a flexible thermoelectric generator in a single run. Our results indicate that III-V nanowire networks directly grown on plastic present a viable route for the facile integration of semiconductor nanowires into flexible large-area thermoelectrics applications.

4. EXPERIMENTAL SECTION

4.1. Nanowire Growth. InAs nanowires were grown directly on polyimide substrates (Polyonics, XT-621) using a metalorganic vapor phase epitaxy system (MOVPE) as discussed in detail in our previous study.[20] Trimethylindium (TMIn) and tertiarybutylarsine (TBAs) were used as precursors and hydrogen was used as a carrier gas with the total reactor gas flow rate of ∼5 L min^{-1} (slm). InAs nanowires were grown from in situ deposited In particles. The growth temperature was varied from 460 to 480 °C with a nominal V/III ratio of 2. The TMIn flow was fixed at 5.95 μmol min^{-1}, and the TBAs flow was set to 12.6 μmol min^{-1}. Total growth time was 2700 s. After the growth, the samples were cooled down under TBAs flow. The growth temperatures reported in this work are thermocouple readings of the lamp-heated graphite susceptor, which are slightly higher than the actual substrate surface temperature.

4.2. Structural Characterization. The nanowire morphology was investigated using scanning electron microscopy (SEM, JEOL JSM-6335F). The network thickness was determined from crosscut SEM images. Prior to imaging, the sample was cast in epoxy resin, grinded, and polished to reveal the cross section, after which a thin Cr layer was sputtered on the surface to reduce the charging of the dielectric epoxy. The crystal structure was investigated using high-resolution transmission electron microscope operated at 200 kV (HRTEM, double aberration-corrected JEOL 2200FS FEG). Elemental composition and the corresponding mapping were determined using TEM-integrated energy-dispersive X-ray spectroscopy (EDS).

4.3. Thermoelectric and Electronic Characterization. The Seebeck coefficient and electrical conductivity were measured using the Linseis LSR-3 measurement system. Ti/Au electrical contacts (20/100 nm) were deposited on the ends of the sample prior measuring. The sample was supported with a glass piece and placed between the electrodes using a thin-film adapter. The measurement was carried out in a helium atmosphere at seven different temperatures between 30 and 210 °C with five different temperature gradients over the sample at each temperature. Four repetitive measurements were made to obtain mean values and standard deviations. Charge carrier concentration and mobility were measured at room temperature using the Ecopia HMS-5300 Hall measurement system. The sample was cut to 10 × 10 mm size, and Ti/Au contacts were deposited to the corners for van der Pauw geometry measurement.

4.4. Mechanical Characterization. The flexibility of the samples was measured using a computer-controlled micrometer stage for bending the sample and a source meter (Keithley 2602B) for recording the current−voltage characteristics at each stage position. The stage was moved forth and back repetitively 1000 times in mechanical stability testing. Prior to measuring, 20/100 nm Ti/Au electrical contacts were deposited at the ends of the sample and the polyimide substrate was carefully stripped off from the carrier glass piece used during the growth step. The sample was connected to the measurement electronics using thin metal wires that were fixed on the contact pads using the Polytec PU-1000 conductive silver epoxy.

4.5. Thermoelectric Generator. The nanowire growth was performed in a similar manner on 8 × 22 mm^2 substrates with polyimide tape masked fractions to define four 8 × 3 mm^2 thermoelectric legs. After the growth, the masking tape was carefully stripped off, the polyimide substrate was carefully removed from the glass support piece, and the electrical connections were defined between different legs using the Polytec PU-1000 conductive silver epoxy. After the interconnections were cured, thin electrical wires were connected at the ends of the device using the same epoxy. The polyimide sheet was then transferred onto a PDMS support piece prepared by mixing (10:1) the PDMS elastomer base and curing agent (Sylgard 184) and baking the mixture poured on a flat surface in an oven at 80 °C for 1 h. Finally, the device was enclosed in PDMS by pouring the same mixture on the device and baking at 80 °C for 1 h.

The performance of the generator was studied by placing it on a hotplate with type K thermocouples fixed on both the hot and the cold ends. The current and voltage characteristics were measured as a function of load resistance for five different temperature gradients.

■ ASSOCIATED CONTENT

Supporting Information

The Supporting Information is available free of charge at https://pubs.acs.org/doi/10.1021/acsaem.1c03405.

TEM and EDS data, additional Seebeck coefficient data, crosscut SEM and nanowire network thickness analysis, and electrical circuit used in generator characterization (PDF)

AUTHOR INFORMATION

Corresponding Author

Tomi Koskinen − *Department of Electronics and Nanoengineering, Aalto University, School of Electrical Engineering, 00076 Aalto, Finland*; orcid.org/0000-0001-6883-4181; Email: tomi.koskinen@aalto.fi

Authors

Vladislav Khayrudinov − *Department of Electronics and Nanoengineering, Aalto University, School of Electrical Engineering, 00076 Aalto, Finland*; orcid.org/0000-0002-4125-6104

Fahimeh Emadi − *Department of Electrical Engineering and Automation, Aalto University, School of Electrical Engineering, 00076 Aalto, Finland*

Hua Jiang − *Department of Applied Physics, Aalto University, School of Science, 00076 Aalto, Finland*

Tuomas Haggren − *Department of Electronics and Nanoengineering, Aalto University, School of Electrical Engineering, 00076 Aalto, Finland; Department of Electronic Materials Engineering, Research School of Physics, The Australian National University, Canberra 2601, Australia*; orcid.org/0000-0001-6033-7391

Harri Lipsanen − *Department of Electronics and Nanoengineering, Aalto University, School of Electrical Engineering, 00076 Aalto, Finland*; orcid.org/0000-0003-2487-4645

Ilkka Tittonen − *Department of Electronics and Nanoengineering, Aalto University, School of Electrical Engineering, 00076 Aalto, Finland*; orcid.org/0000-0002-2985-9789

Complete contact information is available at:
https://pubs.acs.org/10.1021/acsaem.1c03405

Notes

The authors declare no competing financial interest.

ACKNOWLEDGMENTS

T.K. acknowledges Aalto University School of Electrical Engineering Doctoral School and Walter Ahlström Foundation. V.K. acknowledges the support of Aalto University Doctoral School, Walter Ahlström Foundation, Elektroniikkainsinöörien Säätiö, Sähköinsinööriliiton Säätiö, Nokia Foundation, Finnish Foundation for Technology Promotion (Tekniikan Edistämissäätiö), Waldemar Von Frenckell's foundation, and Kansallis-Osake-Pankki fund. T.H. wishes to thank the Finnish Cultural Foundation and Walter Ahlström Foundation for financial support. The Academy of Finland Photonics Flagship PREIN is acknowledged. We acknowledge the provision of facilities and technical support by Aalto University at the Micronova Nanofabrication Centre.

REFERENCES

(1) Barrigón, E.; Heurlin, M.; Bi, Z.; Monemar, B.; Samuelson, L. Synthesis and applications of III−V nanowires. *Chem. Rev.* **2019**, *119*, 9170−9220.

(2) Dayeh, S. A.; Aplin, D. P. R.; Zhou, X.; Yu, P. K. L.; Yu, E. T.; Wang, D. High electron mobility InAs nanowire field-effect transistors. *Small* **2007**, *3*, 326−332.

(3) Tomioka, K.; Yoshimura, M.; Fukui, T. A III−V nanowire channel on silicon for high-performance vertical transistors. *Nature* **2012**, *488*, 189−192.

(4) Saxena, D.; Mokkapati, S.; Parkinson, P.; Jiang, N.; Gao, Q.; Tan, H. H.; Jagadish, C. Optically pumped room-temperature GaAs nanowire lasers. *Nat. Photonics* **2013**, *7*, 963−968.

(5) Wallentin, J.; Anttu, N.; Asoli, D.; Huffman, M.; Åberg, I.; Magnusson, M. H.; Siefer, G.; Fuss-Kailuweit, P.; Dimroth, F.; Witzigmann, B.; Xu, H. Q.; Samuelson, L.; Deppert, K.; Borgström, M. T. InP nanowire array solar cells achieving 13.8% efficiency by exceeding the ray optics limit. *Science* **2013**, *339*, 1057−1060.

(6) Duan, X.; Huang, Y.; Cui, Y.; Wang, J.; Lieber, C. M. Indium phosphide nanowires as building blocks for nanoscale electronic and optoelectronic devices. *Nature* **2001**, *409*, 66−69.

(7) Nadj-Perge, S.; Frolov, S. M.; Bakkers, E. P. A. M.; Kouwenhoven, L. P. Spin−orbit qubit in a semiconductor nanowire. *Nature* **2010**, *468*, 1084−1087.

(8) Albrecht, S. M.; Higginbotham, A. P.; Madsen, M.; Kuemmeth, F.; Jespersen, T. S.; Nygård, J.; Krogstrup, P.; Marcus, C. M. Exponential protection of zero modes in Majorana islands. *Nature* **2016**, *531*, 206−209.

(9) Gül, Ö.; Zhang, H.; Bommer, J. D.; de Moor, M. W.; Car, D.; Plissard, S. R.; Bakkers, E. P.; Geresdi, A.; Watanabe, K.; Taniguchi, T. Ballistic Majorana nanowire devices. *Nat. Nanotechnol.* **2018**, *13*, 192−197.

(10) Hicks, L. D.; Dresselhaus, M. S. Thermoelectric figure of merit of a one-dimensional conductor. *Phys. Rev. B* **1993**, *47*, 16631.

(11) Mingo, N. Thermoelectric figure of merit and maximum power factor in III−V semiconductor nanowires. *Appl. Phys. Lett.* **2004**, *84*, 2652−2654.

(12) Boukai, A. I.; Bunimovich, Y.; Tahir-Kheli, J.; Yu, J.; Goddard, W. A., III; Heath, J. R. Silicon nanowires as efficient thermoelectric materials. *Nature* **2008**, *451*, 168−171.

(13) Hochbaum, A. I.; Chen, R.; Delgado, R. D.; Liang, W.; Garnett, E. C.; Najarian, M.; Majumdar, A.; Yang, P. Enhanced thermoelectric performance of rough silicon nanowires. *Nature* **2008**, *451*, 163−167.

(14) Lohn, A. J.; Coleman, E.; Tompa, G. S.; Kobayashi, N. P. Assessment on thermoelectric power factor in silicon nanowire networks. *Phys. Status Solidi A* **2012**, *209*, 171−175.

(15) Zhang, T.; Wu, S.; Xu, J.; Zheng, R.; Cheng, G. High thermoelectric figure-of-merits from large-area porous silicon nanowire arrays. *Nano Energy* **2015**, *13*, 433−441.

(16) Elyamny, S.; Dimaggio, E.; Magagna, S.; Narducci, D.; Pennelli, G. High power thermoelectric generator based on vertical silicon nanowires. *Nano Lett.* **2020**, *20*, 4748−4753.

(17) Wang, Y.; Yang, L.; Shi, X.-L.; Shi, X.; Chen, L.; Dargusch, M. S.; Zou, J.; Chen, Z.-G. Flexible thermoelectric materials and generators: challenges and innovations. *Adv. Mater.* **2019**, *31*, 1807916.

(18) Bahk, J.-H.; Fang, H.; Yazawa, K.; Shakouri, A. Flexible thermoelectric materials and device optimization for wearable energy harvesting. *J. Mater. Chem. C* **2015**, *3*, 10362−10374.

(19) Du, Y.; Xu, J.; Paul, B.; Eklund, P. Flexible thermoelectric materials and devices. *Appl. Mater. Today* **2018**, *12*, 366−388.

(20) Khayrudinov, V.; Remennyi, M.; Raj, V.; Alekseev, P.; Matveev, B.; Lipsanen, H.; Haggren, T. Direct Growth of Light-Emitting III−V Nanowires on Flexible Plastic Substrates. *ACS Nano* **2020**, *14*, 7484−7491.

(21) Mensch, P.; Karg, S.; Schmidt, V.; Gotsmann, B.; Schmid, H.; Riel, H. One-dimensional behavior and high thermoelectric power factor in thin indium arsenide nanowires. *Appl. Phys. Lett.* **2015**, *106*, No. 093101.

(22) Schmidt, V.; Mensch, P. F. J.; Karg, S. F.; Gotsmann, B.; Das Kanungo, P.; Schmid, H.; Riel, H. Using the Seebeck coefficient to determine charge carrier concentration, mobility, and relaxation time in InAs nanowires. *Appl. Phys. Lett.* **2014**, *104*, No. 012113.

(23) Roddaro, S.; Ercolani, D.; Safeen, M. A.; Suomalainen, S.; Rossella, F.; Giazotto, F.; Sorba, L.; Beltram, F. Giant thermovoltage in single InAs nanowire field-effect transistors. *Nano Lett.* **2013**, *13*, 3638−3642.

(24) Archetti, D.; Neophytou, N. Thermoelectric Properties of InA Nanowires from Full-Band Atomistic Simulations. *Molecules* **2020**, *25*, 5350.

(25) Olsson, L. Ö.; Andersson, C. B. M.; Hākansson, M. C.; Kanski, J.; Ilver, L.; Karlsson, U. O. Charge accumulation at InAs surfaces. *Phys. Rev. Lett.* **1996**, *76*, 3626.

(26) Alekseev, P. A.; Dunaevskiy, M. S.; Cirlin, G. E.; Reznik, R. R.; Smirnov, A. N.; Kirilenko, D. A.; Davydov, V. Y.; Berkovits, V. L. Unified mechanism of the surface Fermi level pinning in III-As nanowires. *Nanotechnology* **2018**, *29*, 314003.

(27) Speckbacher, M.; Treu, J.; Whittles, T. J.; Linhart, W. M.; Xu, X.; Saller, K.; Dhanak, V. R.; Abstreiter, G.; Finley, J. J.; Veal, T. D.; Koblmüller, G. Direct measurements of Fermi level pinning at the surface of intrinsically n-type InGaAs nanowires. *Nano Lett.* **2016**, *16*, 5135−5142.

(28) Weber, J. R.; Janotti, A.; van de Walle, C. G. Intrinsic and extrinsic causes of electron accumulation layers on InAs surfaces. *Appl. Phys. Lett.* **2010**, *97*, 192106.

(29) Degtyarev, V. E.; Khazanova, S. V.; Demarina, N. V. Features of electron gas in InAs nanowires imposed by interplay between nanowire geometry, doping and surface states. *Sci. Rep.* **2017**, *7*, 1−9.

(30) Rogalski, A.; Jóźwikowski, K. Intrinsic carrier concentration and effective masses in InAs1− xSbx. *Infrared Phys.* **1989**, *29*, 35−42.

(31) Kamp, M.; Weyers, M.; Heinecke, H.; Lüth, H.; Balk, P. MOMBE of InAs on GaAs. *J. Cryst. Growth* **1990**, *105*, 178−184.

(32) Thelander, C.; Dick, K. A.; Borgström, M. T.; Fröberg, L. E.; Caroff, P.; Nilsson, H. A.; Samuelson, L. The electrical and structural properties of n-type InAs nanowires grown from metal−organic precursors. *Nanotechnology* **2010**, *21*, 205703.

(33) Fang, Z. M.; Ma, K. Y.; Cohen, R. M.; Stringfellow, G. B. Effect of growth temperature on photoluminescence of InAs grown by organometallic vapor phase epitaxy. *Appl. Phys. Lett.* **1991**, *59*, 1446−1448.

(34) Kim, H.-S.; Gibbs, Z. M.; Tang, Y.; Wang, H.; Snyder, G. J. Characterization of Lorenz number with Seebeck coefficient measurement. *APL Mater.* **2015**, *3*, No. 041506.

(35) Park, S.-I.; Ahn, J.-H.; Feng, X.; Wang, S.; Huang, Y.; Rogers, J. A. Theoretical and experimental studies of bending of inorganic electronic materials on plastic substrates. *Adv. Funct. Mater.* **2008**, *18*, 2673−2684.

(36) Tian, Y.; Sakr, M. R.; Kinder, J. M.; Liang, D.; MacDonald, M. J.; Qiu, R. L. J.; Gao, H.; Gao, X. P. A. One-dimensional quantum confinement effect modulated thermoelectric properties in InAs nanowires. *Nano Lett.* **2012**, *12*, 6492−6497.

(37) Mensch, P.; Karg, S.; Gotsmann, B.; Kanungo, P. D.; Schmidt, V.; Troncale, V.; Schmid, H.; Riel, H. Electrical and thermoelectrical properties of gated InAs nanowire, In *Proceedings of the European Solid-State Device Research Conference (ESSDERC) 2013*; IEEE: 2013; pp. 252−255.

(38) Karg, S.; Schaller, V.; Gaul, A.; Moselund, K.; Schmid, H.; Gotsmann, B.; Gooth, J.; Riel, H. Ballistic transport and high thermopower in one-dimensional InAs nanowires, In *46th European Solid-State Device Research Conference (ESSDERC) 2016*; IEEE: 2016; pp. 341−344.

(39) Jeon, S. G.; Park, D. W.; Shin, H. S.; Park, H. M.; Choi, S. Y.; Lee, S. J.; Yu, J.; Song, J. Y. Effects of doping and planar defects on the thermoelectric properties of InAs nanowires. *RSC Adv.* **2016**, *6*, 7791−7797.

(40) Paul, B.; Björk, E. M.; Kumar, A.; Lu, J.; Eklund, P. Nanoporous Ca3Co4O9 thin films for transferable thermoelectrics. *ACS Appl. Energy Mater.* **2018**, *1*, 2261−2268.

(41) Hollar, C.; Lin, Z.; Kongara, M.; Varghese, T.; Karthik, C.; Schimpf, J.; Eixenberger, J.; Davis, P. H.; Wu, Y.; Duan, X.; Zhang, Y.; Estrada, D. High-performance flexible bismuth telluride thin film from solution processed colloidal nanoplates. *Adv. Mater. Technol.* **2020**, *5*, 2000600.

(42) Feng, J.; Zhu, W.; Deng, Y.; Song, Q.; Zhang, Q. Enhanced antioxidation and thermoelectric properties of the flexible screen-printed Bi2Te3 films through interface modification. *ACS Appl. Energy Mater.* **2019**, *2*, 2828−2836.

(43) Gao, Q.; Wang, W.; Lu, Y.; Cai, K.; Li, Y.; Wang, Z.; Wu, M.; Huang, C.; He, J. High Power Factor Ag/Ag2Se Composite Films for Flexible Thermoelectric Generators. *ACS Appl. Mater. Interfaces* **2021**, *13*, 14327−14333.

(44) Roslyak, O.; Piryatinski, A. Thermoelectric properties of semiconductor nanowire networks. *J. Appl. Phys.* **2016**, *119*, 125107.

(45) Zhou, F.; Moore, A. L.; Bolinsson, J.; Persson, A.; Fröberg, L.; Pettes, M. T.; Kong, H.; Rabenberg, L.; Caroff, P.; Stewart, D. A.; Mingo, N.; Dick, K. A.; Samuelson, L.; Linke, H.; Shi, L. Thermal conductivity of indium arsenide nanowires with wurtzite and zinc blende phases. *Phys. Rev. B* **2011**, *83*, 205416.

(46) Persson, A. I.; Koh, Y. K.; Cahill, D. G.; Samuelson, L.; Linke, H. Thermal conductance of InAs nanowire composites. *Nano Lett.* **2009**, *9*, 4484−4488.

(47) Ren, P.; Zhu, X.; Han, J.; Xu, J.; Ma, L.; Li, H.; Zhuang, X.; Zhou, H.; Zhang, Q.; Xia, M.; Pan, A. Synthesis and diameter-dependent thermal conductivity of InAs nanowires. *Nano-Micro Letters* **2014**, *6*, 301−306.

(48) Rocci, M.; Demontis, V.; Prete, D.; Ercolani, D.; Sorba, L.; Beltram, F.; Pennelli, G.; Roddaro, S.; Rossella, F. Suspended InAs Nanowire-Based Devices for Thermal Conductivity Measurement Using the 3ω Method. *J. Mater. Eng. Perform.* **2018**, *27*, 6299−6305.

(49) Swinkels, M. Y.; van Delft, M. R.; Oliveira, D. S.; Cavalli, A.; Zardo, I. v.; van der Heijden, R. W.; Bakkers, E. P. A. M. Diameter dependence of the thermal conductivity of InAs nanowires. *Nanotechnology* **2015**, *26*, 385401.

(50) Juntunen, T.; Koskinen, T.; Khayrudinov, V.; Haggren, T.; Jiang, H.; Lipsanen, H.; Tittonen, I. Thermal conductivity suppression in GaAs−AlAs core−shell nanowire arrays. *Nanoscale* **2019**, *11*, 20507−20513.